# CO oxidation catalyzed by Cu-exchanged zeolites: a density functional theory study

D. Sengupta [a], W.F. Schneider [b], K.C. Hass [b] and J.B. Adams [a]

[a] *Department of Chemical, Bio and Materials Engineering, Arizona State University, Tempe, AZ 85287, USA*
[b] *Ford Research Laboratory, MD 3028/SRL, Dearborn, MI 48121-2053, USA*

Received 11 May 1999; accepted 9 July 1999

The catalytic oxidation of CO by Cu-exchanged high-silica zeolites (e.g., ZSM-5) has been investigated theoretically using density functional theory. Calculations reveal two distinct, parallel pathways for oxidation of CO: (i) adsorption of $O_2$ on a reduced Cu site followed by O atom abstraction by CO, and (ii) adsorption of CO followed by its reaction with $O_2$ to form a cyclic compound which decomposes to form $CO_2$. The reduced site is regenerated via two different pathways, both of which involve oxidation of one or more CO molecules: (i) abstraction of atomic oxygen by CO from the oxidized active site, and (ii) formation of a carbonate species followed by its reaction with a molecule of CO. The relevance of these reactions to the reduction of NO is discussed.

**Keywords:** CO oxidation, Cu-ZSM-5, zeolites, DFT

## 1. Introduction

Current interest in "lean-burn" engines for automobiles has spurred efforts to develop catalysts capable of reducing $NO_x$ in the oxygen-rich exhaust they produce [1–3]. Traditional three-way catalysts (TWCs), i.e, supported Rh, Pd and Pt, are highly effective for treating the exhaust produced during stoichiometric combustion, but rapidly lose this activity in increasingly lean fuel/air mixtures [4]. Ion-exchanged zeolites, especially Cu-ZSM-5, have garnered considerable attention for their ability to promote the selective catalytic reduction of $NO_x$ by hydrocarbons in an $O_2$-rich environment. While these same materials also catalyze the reduction of $NO_x$ by CO, this activity is poisoned by $O_2$, presumably because of competition with catalytic CO oxidation [2,3]:

$$2CO + O_2 \rightarrow 2CO_2 \tag{1}$$

Because of the central importance of catalytic CO oxidation in automotive catalysis, and the relevance of the CO chemistry to $NO_x$ reduction, we have undertaken a theoretical examination of CO oxidation in Cu-zeolites using first-principles density functional theory (DFT).

The catalytic oxidation of CO to $CO_2$ is a key feature of TWC chemistry, and its reaction mechanism on noble metal surfaces has been extensively investigated [5–7]. The reaction is described by a Langmuir–Hinshelwood mechanism: CO and $O_2$ co-adsorb on the surface, the latter dissociatively, and through surface diffusion combine to produce $CO_2$ [8]. This mechanism hinges on the availability of very many closely spaced surface sites able to accommodate CO and atomic oxygen. Such is not the case in high-silica Cu-exchanged zeolites: the Cu ion active sites are on average rather widely separated, making reactions (including $O_2$ dissociation and CO + O recombination) involving multiple Cu sites unlikely. In previous work on the Cu-zeolite-catalyzed NO oxidation, we have proposed an Eley–Rideal mechanism in which $O_2$ is adsorbed and effectively dissociated in multiple steps on a single Cu active site ("ZCu") [9,10]:

$$ZCu + O_2 \rightarrow ZCuO_2 \tag{2}$$

$$ZCuO_2 + NO \rightarrow ZCuO + NO_2 \tag{3}$$

$$ZCuO + NO \rightarrow ZCuONO \tag{4}$$

$$ZCuONO \rightleftharpoons ZCu + NO_2 \tag{5}$$

In this work, we apply the same isolated active site model to the catalytic oxidation of CO in Cu-zeolites. We find a CO oxidation pathway that closely parallels that proposed for NO, modified by the greater reducing power of CO, and augmented by a number of additional pathways, in particular one which involves formation and decomposition of a carbonate intermediate. These model results account for the facile oxidation of CO in Cu-ZSM-5, and provide some insight into the mechanism of the non-selective reduction of NO by CO.

One of the main challenges of the first-principles modeling of Cu-zeolite catalysis is representation of the active site. Previous theoretical [11–18] and experimental [19–21] work has demonstrated that exchanged $Cu^+$ ions prefer a low-coordination environment within a zeolite, and that this coordination environment is well represented by a single, framework Al tetrahedral (T-) site in which the Al–O–H groups represent Al–O–Si linkages in the zeolite:

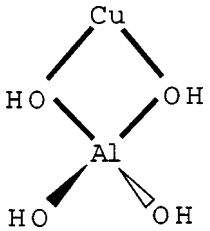


The formally anionic $Al(OH)_4^-$ fragment ("Z") charge compensates the $Cu^+$ center to yield an overall charge-neutral cluster. This model has been quite successful in describing the binding, spectroscopy, and reactivity of adsorbates, yielding nearly quantitative agreement with the predictions of more elaborate zeolite models [9–13]. We employ this single T-site model in all the calculations reported here.

## 2. Computational details

DFT calculations were performed using the Amsterdam Density Functional code (ADF) [22]. Geometry optimizations and vibrational frequencies were determined within the local (spin) density approximation [L(S)DA]. Single point energy calculations were performed on the L(S)DA optimized geometries with the Becke–Perdew exchange correlation functional (BP86) [23,24]. A valence double-$\zeta$ plus polarization Slater-type basis set was used for all atoms save Cu, for which a double-$\zeta$ s, p and triple-$\zeta$ d basis set was used. Integration parameters were chosen to ensure that numerically evaluated integrals are accurate to five significant digits. Geometries were converged to maximum and root mean square gradients of $10^{-3}$ and $6.6 \times 10^{-4}$ hartree bohr$^{-1}$, respectively, and energies to less than $10^{-5}$ hartree. Vibrational spectra were calculated by two-sided numerical differentiation of analytical energy gradients. Minimum energy and transition state structures were characterized by zero and one imaginary vibrational frequency, respectively.

## 3. Results

### *3.1. Adsorption of CO, $O_2$, and $CO_2$ on ZCu*

Adsorption of reactants and desorption of products are fundamental steps in any heterogeneous catalytic process. We begin by summarizing new and previously obtained results for adducts of CO, $O_2$, and $CO_2$ with a Cu(I) (ZCu) site in a Cu-exchanged zeolite.

Adsorption of CO has been studied extensively as a probe of the existence and nature of ZCu sites [21,25,26]. Formation of monocarbonyls (ZCuCO) occurs readily on these sites and in Cu-ZSM-5 is accompanied by a slight ($\sim$15 cm$^{-1}$) blue shift in the characteristic C–O stretch mode. A similar trend was also obtained for Cu-zeolite-Y [27]. Electronic structure calculations using a variety of zeolite models, including the single T-site one considered here, are in agreement that CO binds linearly to ZCu (figure 1, **A**) with a binding energy of approximately 40 kcal mol$^{-1}$ [9,13]. The C–O bond length and stretch frequency are more sensitive functions of the Lewis basicity of the "Z" model (or of the actual zeolite coordination site), weaker bases decreasing and stronger bases lengthening the C–O bond compared to free CO [11–13]. Because of its high basicity, the single T-site model predicts the C–O bond to be lengthened by 0.01 Å and the C–O stretch to be red-shifted.

Dicarbonyl complexes can be formed in Cu-ZSM-5 by the further addition of CO to ZCuCO [21]:

$$\mathrm{ZCuCO} + \mathrm{CO} \rightleftharpoons \mathrm{ZCu(CO)_2} \qquad (6)$$

In agreement with earlier computational work, we find the dicarbonyl to have pseudotetrahedral symmetry about the Cu center (figure 1, **B**). The calculated C–Cu–C angle is 119.9° and both carbonyl groups bind in an almost linear fashion to the Cu. The Cu–C bond lengths (1.828 and 1.866 Å vs. 1.750 Å) are longer and the C–O distances are slightly shorter in the dicarbonyl than the monocarbonyl complex due to greater competition for back-donated metal electrons in the former case. The symmetric and antisymmetric stretching vibrations are predicted to occur at 2122 and 2167 cm$^{-1}$, which compare well with the experimental values of 2151 and 2178 cm$^{-1}$ [28,29]. While Cu-dicarbonyls are known to be quite stable [21,29], reaction (6) is only 7 kcal mol$^{-1}$ exothermic in the single T-site model. The addition of two CO strongly reduces the Cu center and likely favors a less basic environment for the Cu than that provided by the single T-site model.

In contrast to CO, little is known about the adsorption of $O_2$ or $CO_2$ on ZCu. Previous theoretical work supports the existence of a one-to-one adduct of $O_2$ with ZCu [9] with a binding energy somewhat less than that of CO. This $ZCuO_2$ adduct takes two isomeric forms: a bidentate one (figure 1, **C**) with a binding energy of 30 kcal mol$^{-1}$, and a monodentate one (figure 1, **D**) with a binding energy 6 kcal mol$^{-1}$ less. Thus, while similar in connectivity to peroxide and superoxide $O_2$ complexes, the $ZCuO_2$ isomers have many characteristics of a simple coordination complex between $O_2$ and Cu(I). The calculated O–O bond lengths are increased by only 0.08 and 0.05 Å, respectively, over that in molecular $O_2$ (1.218 Å). Like molecular $O_2$, both isomers are paramagnetic and have a triplet ground state, with unpaired spin density mostly localized on the two O atoms. As has been shown previously [15] and will be demonstrated again below, adsorption on ZCu activates $O_2$ for further chemistry.

Like $O_2$, $CO_2$ is predicted to form both bi- (side-on) (figure 1, **E**) and monodentate (end-on) (figure 1, **F**) one-to-one adducts with ZCu. Only side-on binding was found in Hartree–Fock calculations for $CO_2$ adsorption on $Cu(PH_3)^+$ [30], but both binding modes were found in higher level calculations for other Cu–$CO_2$ complexes [31]. Our predicted binding energies for bi- and monodentate adsorption of $CO_2$ on ZCu (10 and 8 kcal mol$^{-1}$, respectively) are much smaller than those for CO or $O_2$. Coordination

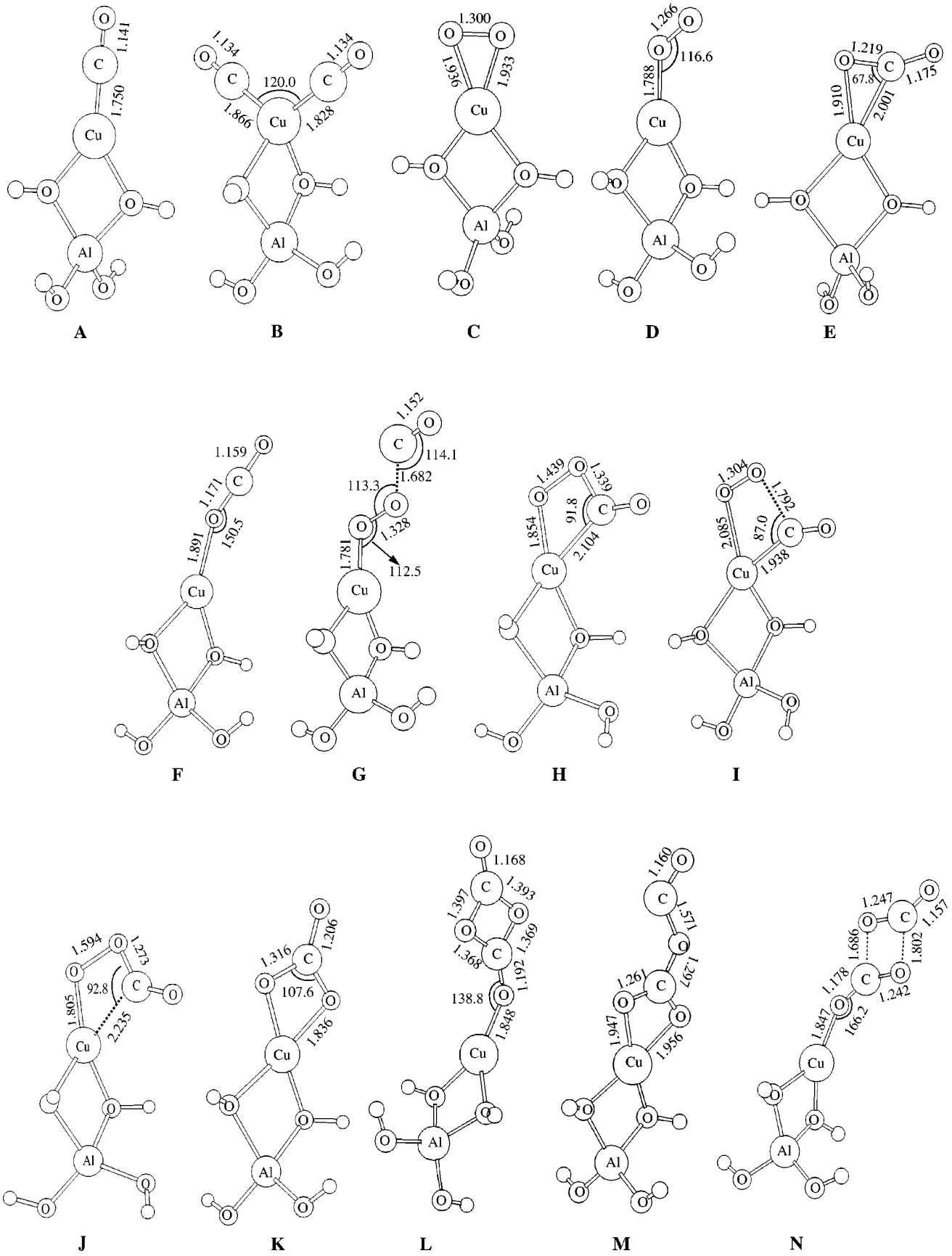


Figure 1. Selected geometrical parameters of all equilibrium and transition structures considered. Bond lengths and bond angles are in ångstroms and degrees, respectively. **A–F, H, K, L** are equilibrium structures and **G, I, J, M, N** are transition structures.

to the Cu(I) center is accompanied by weak charge transfer to $CO_2$, which induces a slight increase in C–O bond lengths (by 0.01–0.05 Å compared to our calculated gas-phase value of 1.164 Å) and changes in symmetric and antisymmetric C–O stretching frequencies. We calculate these frequencies to be 1355 and 2428 $cm^{-1}$, respectively, in the gas phase, with shifts of $-141$ and $-271$ $cm^{-1}$ in the bidendate isomer, and $-23$ and $+7$ $cm^{-1}$ in the monodentate isomer. The slight blue shift of the antisymmetric mode in the latter isomer corresponds exactly to the value assigned to weakly adsorbed $CO_2$ in Cu-ZSM-5 on the basis of infrared measurements in the presence of CO [28].

These adsorbed molecules constitute the first step in the catalytic oxidation of CO. In the following section we will investigate oxidation of CO by two different paths: abstraction of O by CO from $ZCuO_2$ and addition of $O_2$ to ZCuCO followed by its decomposition.

### 3.2. $O_2$ cleavage reactions

In the catalytic NO oxidation chemistry previously studied (reactions (2)–(5)), oxidation begins with adsorption of $O_2$ in the monodentate form (reaction (2)) and subsequent O-atom abstraction by reaction with gas-phase NO (reaction (3)), leaving behind an oxidized ZCu site, i.e., ZCuO. Like $ZCuO_2$, ZCuO has a triplet ground state with unpaired spin density mostly residing on the O atom. The abstraction reaction is exothermic by 7 kcal $mol^{-1}$ in the single T-site model [9]. This reaction proceeds via an intermediate complex, $ZCuOO\cdots NO$, 10 kcal $mol^{-1}$ more stable than the separate reactants, which dissociates into $ZCuO + NO_2$.

We have examined the analogous reaction of CO with adsorbed $O_2$:

$$ZCuO_2 + CO \rightleftharpoons ZCuO + CO_2 \quad (7)$$

As shown in figure 2, reaction (7) is highly exothermic (55 kcal $mol^{-1}$) and proceeds with an activation barrier of 17 kcal $mol^{-1}$. However, we did not find any intermediate complex $ZCuOO\cdots CO$. The "O–O–C–O" unit is essentially planar at the transition state, and both *cis* and *trans* orientations are of comparable energy. In the *trans* transition state (figure 1, **G**) the O–O bond length is increased slightly from its initial value (1.266 to 1.329 Å), while the forming C–O bond distance is rather large (1.682 Å). The transition state is "early", consistent with the high reaction exothermicity.

An alternative mechanism, possibly favored by the higher adsorption energy of CO than $O_2$, involves initial adsorption of CO followed by reaction with gas-phase $O_2$:

$$ZCuCO + O_2 \rightarrow ZCuO + CO_2 \quad (8)$$

The analogous NO reaction is endothermic by 9 kcal $mol^{-1}$ in the single T-site model and is not believed to occur [9]. As shown in figure 2, reaction (8) is both exothermic (37 kcal $mol^{-1}$) and proceeds by a two-step mechanism. In the first step, $O_2$ binds to ZCuCO to form a cyclic triplet

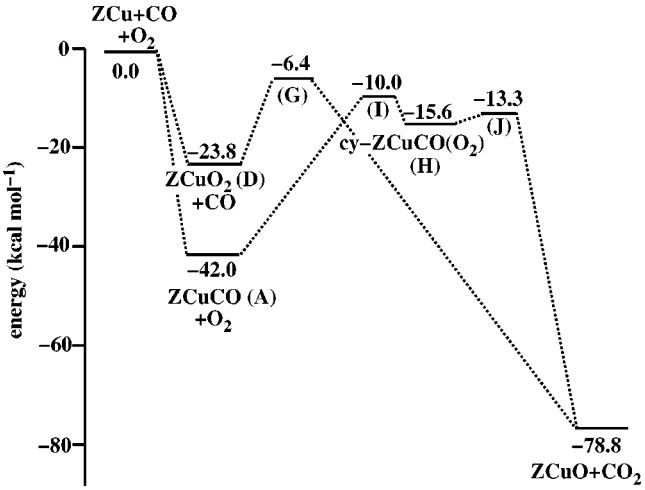


Figure 2. Schematic potential energy surfaces for two different pathways for ZCu + CO + $O_2$ reactions. Letters within parentheses refer to the structures shown in figure 1.

intermediate (figure 1, **H**). This intermediate then dissociates into ZCuO and $CO_2$:

$$ZCuCO + O_2 \rightarrow TS1 \rightarrow cy\text{-}ZCuCO(O_2) \quad (9)$$

$$cy\text{-}ZCuCO(O_2) \rightarrow TS2 \rightarrow ZCuO + CO_2 \quad (10)$$

The triplet four-membered cyclic intermediate lies about 26 kcal $mol^{-1}$ above the separated ZCuCO + $O_2$, and 20 kcal $mol^{-1}$ above its corresponding singlet ground state. It is characterized by relatively longer O–O and O–C lengths compared to those in free $O_2$ and $CO_2$, respectively. The formation of the cyclic intermediate from ZCuCO and $O_2$ (reaction (9)) has a barrier of 32 kcal $mol^{-1}$. The transition state for this process and reaction (10) are shown in figure 1 (**I** and **J**, respectively). The intermediate complex, **H**, dissociates into ZCuO + $CO_2$ with an activation barrier of approximately 2 kcal $mol^{-1}$ and is expected to be extremely short lived. The transition state for reaction (9) has longer Cu–O and O–C distance relative to those in **H**. A normal mode analysis confirms that the imaginary mode involves a concerted motion coupling H to the reactants, ZCuCO + $O_2$. On the other hand, the transition state for reaction (10) has longer O–O and Cu–C lengths compared to those in **H**; its imaginary frequency mode corresponds to a concerted motion in which these two bonds stretch in-phase, while the corresponding Cu–O and O–C bonds stretch with the opposite phase.

### 3.3. Regeneration of reduced sites, ZCu

The above reactions represent the first half of a catalytic CO oxidation cycle; they produce oxidized ZCuO sites which must be reduced by a second CO molecule. The most direct route is addition of CO to form adsorbed $CO_2$, followed by $CO_2$ desorption:

$$ZCuO + CO \rightarrow ZCuCO_2 \quad (11)$$

$$ZCuCO_2 \rightarrow ZCu + CO_2 \quad (12)$$

While the first step is highly exothermic (79 kcal mol$^{-1}$), it is "spin-forbidden", i.e., spin-triplet reactants (ZCuO + CO) evolve into spin-singlet products ($ZCuCO_2$). The triplet to singlet interconversion occurs at a "crossing point" along the reaction coordinate, which, while analogous to a transition state for a spin-allowed reaction, cannot be found by normal transition state searching techniques. However, an approximate activation barrier can be obtained by identifying the lowest energy point of intersection of the triplet and the singlet potential energy surfaces. We take this approach here.

To locate a crossing point, we calculate the energy of the appropriate triplet state as a function of ZCuO–CO distance, from 3.0 to 1.3 Å, relaxing all other geometric parameters save the $Al(OH)_4$ "framework" (figure 3). Optimizing the other parameters ensures that the system is close to the minimum energy path. The energy of the singlet state at each of these triplet-optimized geometries was then determined. The approximate activation energy is obtained from the crossing point of the singlet and triplet potential energy curves, which provides an upper limit to the "true" crossing energy. The estimated activation barrier from the crossing point is 9 kcal mol$^{-1}$. At the crossing point (the approximate transition structure), the ZCuO–CO distance is 1.943 Å while the ZCu–OCO distance is 1.705 Å. Along this reaction path, the carbon atom gradually moves towards Cu, and finally forms the bidentate $ZCuCO_2$ complex. Carbon dioxide can then desorb to regenerate the reduced site, ZCu.

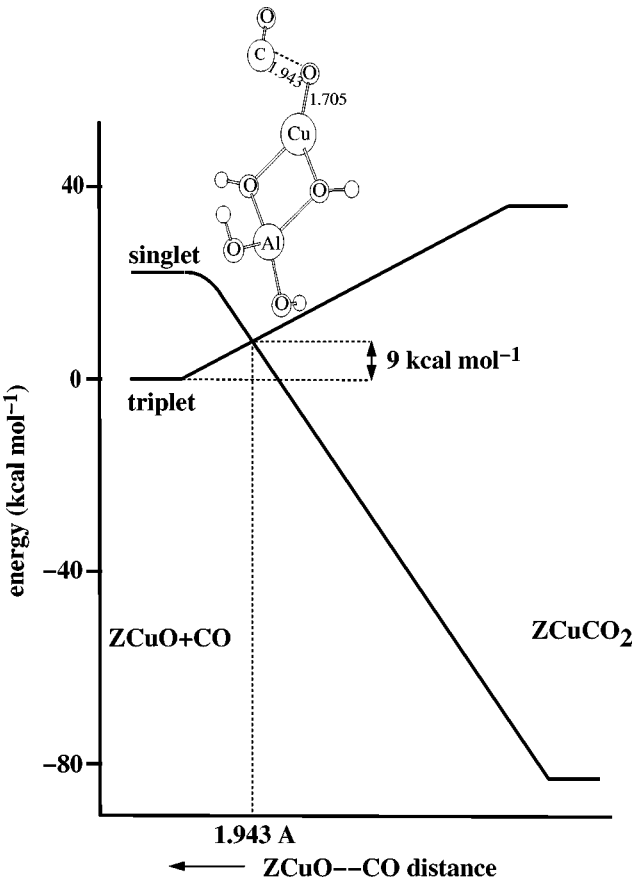


Figure 3. Schematic potential energy surfaces for singlet and triplet states of the reaction ZCuO + CO → $ZCuCO_2$. The crossing point of the two curves indicates the approximate position of the transition state. The structure at the crossing point is also shown. Note that ZCuO–CO distance decreases from left to right.

### 3.4. Formation and decomposition of the carbonate $ZCuCO_3$

Reactions (11) and (12) complete a mechanism for catalytic CO oxidation over Cu-exchanged zeolite catalysts which essentially parallels that described previously for NO oxidation. We now consider a pathway via a carbonate intermediate $ZCuCO_3$ (see figure 1, **K**), which does not have a direct analog to the mechanisms considered previously. A carbonate species, $ZCuCO_3$ could be formed by at least two different pathways:

$$ZCu\left(\eta^2\text{-}O_2\right) + CO \rightarrow ZCuCO_3 \quad (13)$$

$$ZCuO + CO_2 \rightarrow ZCuCO_3 \quad (14)$$

Both of these reactions are spin-forbidden. Reaction (13) is exothermic by 88 kcal mol$^{-1}$. We used techniques similar to those discussed above to locate the crossing point for reaction (13). The reaction coordinate in this case was chosen to be the distance between the midpoint of the O–O bond and the carbon of CO. The path necessitates the rupture of the strong O–O bond, and as a result the crossing point is 100 kcal mol$^{-1}$ above the reactants. We conclude that this reaction is unlikely to contribute to $ZCuCO_3$ formation.

In contrast, reaction (14) is only 33 kcal mol$^{-1}$ exothermic but has a much lower activation energy. For reaction (14), we chose a somewhat more complicated reaction coordinate, starting from $ZCuCO_3$, and moving $CO_2$ away in such a manner that ZCuO and $CO_2$ gradually relax to their equilibrium geometries. It should be noted that changes in geometrical parameters leading to their equilibrium geometries were done manually instead of by optimization due to an SCF convergence problem during optimization. Using this procedure, we find a crossing point only 15 kcal mol$^{-1}$ above the reactants (figure 4), indicating that formation of the carbonate should occur readily via this pathway. The two forming ZCu(O)–OCO and ZCuO–C(O)O bonds at the crossing point are 2.295 and 1.810 Å, respectively, and the ZCu–OC(O)O bond is 1.793 Å. Formation of the analogous carbonate intermediate was proposed to be one of the pathways of CO oxidation over Ag metal [34]. The carbonate species on the Ag surface was claimed to be formed by a reaction between adsorbed CO and molecular oxygen. However, we found this mechanism in Cu-ZSM-5 to be unlikely, while the reaction between ZCuO and $CO_2$ (reaction (14)) is reasonably favorable.

$ZCuCO_3$ has a square planar coordination about the Cu center (figure 1, **K**). Both the Cu-bound O–C lengths are 1.836 Å, while the terminal C–O length is 1.206 Å. Carbonate is formally dianionic, and as such strongly oxidizes

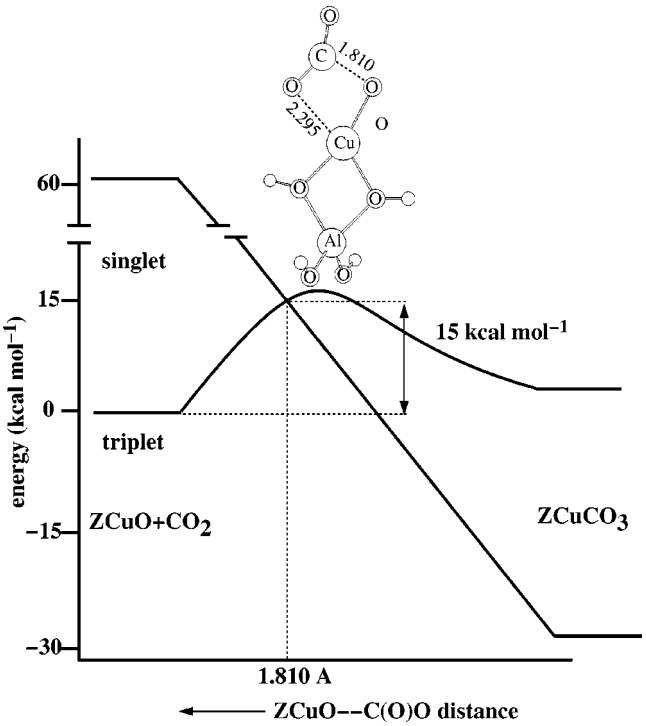


Figure 4. Schematic potential energy surfaces for singlet and triplet states of the reaction $ZCuO + CO_2 \rightarrow ZCuCO_3$. The crossing point of the two curves indicates the approximate position of the transition state. The structure at the crossing point is also shown. Note that ZCuO–C(O)O distance decreases from left to right.

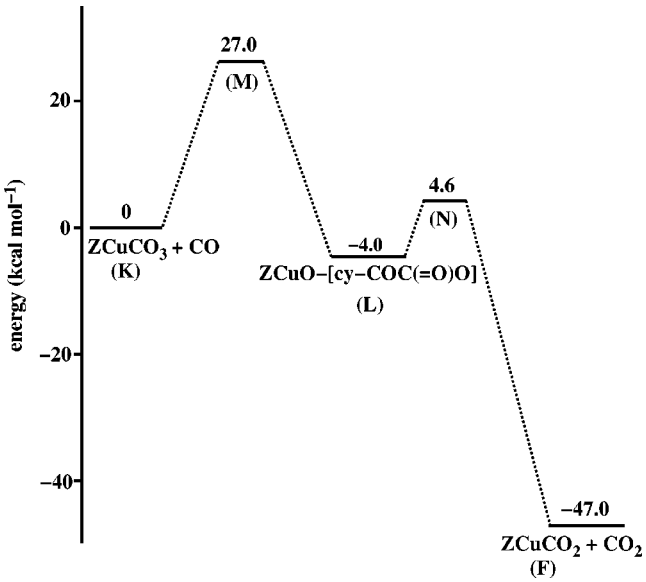


Figure 5. Schematic potential energy surface for the reaction $ZCuCO_3 + CO \rightarrow ZCuCO_2 + CO$. Letters within parentheses refer to the structures shown in figure 1.

the Cu center: the electronic structure is best represented as ZCu(III)–$CO_3^{2-}$, with a singlet ground state. The calculated vibrational spectrum of $ZCuO_3$ includes intense bands at 1741 and 1258 $cm^{-1}$ corresponding to the C=O stretch and C–O antisymmetric stretch, respectively, and weaker bands at 1023 (C–O symmetric stretch), 778 (umbrella), 674 (symmetric bend) and 638 $cm^{-1}$ (asymmetric bend). These values are typical of those observed for bidentate carbonate complexes [32]. To our knowledge, the carbonate $ZCuCO_3$ has not been investigated spectroscopically in Cu-exchanged zeolites, although these results indicate that it should be readily observed.

While direct $CO_2$ loss from $ZCuCO_3$ is energetically unfavorable, the carbonate can be decomposed by reaction with an additional CO molecule:

$$ZCuCO_3 + CO \rightarrow ZCuCO_2 + CO_2 \qquad (15)$$

Reaction (15) is exothermic by 47 kcal $mol^{-1}$ and is spin-allowed. However, this reaction does not proceed via a direct abstraction of the C=O oxygen of $ZCuCO_3$. Reaction (15) is actually a two-step process:

$$ZCuCO_3 + CO \rightarrow ZCuO[cy\text{-}COC(=O)O] \qquad (16)$$

$$ZCuO[cy\text{-}COC(=O)O] \rightarrow ZCuCO_2 + CO_2 \qquad (17)$$

The first step (reaction (16)) is exothermic by approximately 4 kcal $mol^{-1}$ with an activation barrier of 26 kcal $mol^{-1}$ (figure 5). The existence of the four-membered ring structure (figure 1, **L**) was traced by reaction path calculation as a function of $ZCuO_2CO$–CO distance while optimizing all other geometrical parameters. The Cu center in the four-membered ring species is highly reduced with a d-electron population of 9.72. This species, therefore, can be represented as ZCu(I)–[cy-COC(=O)O]. The four-membered ring is essentially planar. The transition state of reaction (16) is shown in figure 1, **M**. The two Cu–O bonds in the $CO_3$ portion appear to be almost symmetric with one of them being slightly longer than the other (by 0.01 Å). The $ZCuO_2CO$–CO length is 1.580 Å, while the $ZCuO_2C$–OCO bond is stretched only by 0.085 Å from its value in $ZCuCO_3$. The normal mode analysis of the imaginary frequency shows that one of the Cu–O bonds tends to break as CO approaches closer. However, our reaction path calculations confirm the formation of the four-membered ring structure.

In the second step (reaction (17)), the four-membered ring dissociates to produce $ZCuCO_2$ and $CO_2$ (figure 5). This reaction is exothermic by 43 kcal $mol^{-1}$ with an activation barrier of only 8.6 kcal $mol^{-1}$. At the transition state (figure 1, **N**), the two C–O bonds of the four-membered ring are stretched by approximately 0.4 and 0.3 Å, while the Cu–O–C angle is widened by approximately 28°. The normal mode corresponding to the imaginary frequency clearly shows a symmetric stretching motion of the two stretched C–O bonds in the ring.

Reactions (14) and (15) provide an alternative to the direct reaction of ZCuO with CO (reaction (11)) for the reduction of ZCuO. Reactions (11) and (14) are both spin-forbidden, but have comparable estimated activation energies. We expect both reactions to be roughly competitive with one another kinetically. Subsequent decomposition of $ZCuCO_3$ by reactions (16) and (17) has a somewhat higher activation energy, but should still occur readily. Thus, we

expect that, under CO oxidation conditions, both pathways will operate in the reduction of ZCuO to ZCu.

## 4. Discussion

Figure 6 summarizes the reactions studied here in the form of a catalytic cycle. CO oxidation is accomplished by cycling between reduced (ZCu) and oxidized (ZCuO) Cu states. The ZCu → ZCuO conversion can occur by preadsorption of either $O_2$ or CO on ZCu, followed by an Eley–Rideal type reaction with the other partner (reactions (7) and (8)). The modeling results indicate that both of these occur with similar rates, although preadsorption of CO is more energetically favored.

The reverse conversion of ZCuO → ZCu is possible via two pathways: a direct reaction with CO to produce $CO_2$ (reactions (11) and (12)) or a somewhat more complicated pathway involving formation and decomposition of a carbonate intermediate (reactions (14), (15), and (12)). Both pathways involve a "spin-forbidden" step, but ones with apparently low singlet–triplet crossing points and thus small activation barriers. Direct calculation of the rate of spin-forbidden reactions for polyatomic systems remains a considerable computational challenge (see, for instance, [37]). However, because our estimates of the barriers for both reactions are low (9 and 15 kcal mol$^{-1}$, respectively), it seems likely that one, if not both, of these pathways is readily accessible. In summary, the model results are consistent with a facile catalytic oxidation of CO by Cu-exchanged zeolites, and provide a reasonable mechanism for this process.

To understand the mechanism of the catalytic reduction process of NO, Iwamoto and Hamada [2] carried out controlled experiments in the presence and absence of oxygen using CO as the reductant. While a marked increase in NO to $N_2$ conversion was observed with CO as the reductant, addition of excess $O_2$ drastically decreased the catalytic activity.

The present and previously reported [10] results suggest one mechanism for the reduction of NO by CO. NO decomposition in Cu-ZSM-5 has been proposed to proceed by a two-step mechanism [10], the first of which yields $N_2O$ by oxidation of a ZCu site:

$$\mathrm{ZCu} + 2\mathrm{NO} \rightarrow \mathrm{ZCuO} + \mathrm{N_2O} \tag{18}$$

and the second of which produces $N_2$ either by reaction with ZCuO or ZCu:

$$\mathrm{ZCuO} + \mathrm{N_2O} \rightarrow \mathrm{ZCu} + \mathrm{N_2} + \mathrm{O_2} \tag{19}$$

$$\mathrm{ZCu} + \mathrm{N_2O} \rightarrow \mathrm{ZCuO} + \mathrm{N_2} \tag{20}$$

While reactions (18) and (19) constitute a complete catalytic cycle, reactions (18) and (20) do not. Instead, reaction (20) and other more complex, but potentially more favorable [35], mechanisms for producing $N_2$ from $N_2O$, require a secondary reductant to regenerate a reduced Cu site. The present work has shown that CO readily converts ZCuO to ZCu via reactions (11) and (12). Thus, if reactions that oxidize the Cu site (e.g., reaction (20)) outcompete reaction (19) under certain conditions, CO may simply drive NO reduction forward by regenerating ZCu in these cases. In addition, CO may play a more direct role by reacting with various N-containing Cu complexes; a detailed examination of such reactions in high-silica Cu zeolites will be presented elsewhere [35].

Because both CO and NO bind more strongly to reduced sites than does $O_2$, a simple blocking mechanism cannot fully account for inability of CO to *selectively* reduce NO in the presence of excess $O_2$. Rather, this inability may have its origins in the dynamic balance established

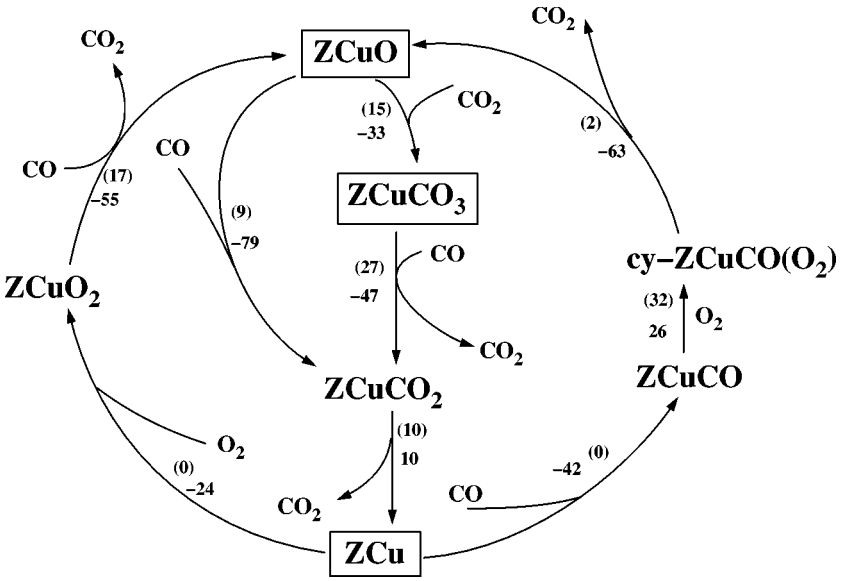


Figure 6. The catalytic cycle for CO oxidation combining the reactions presented in figures 2–5. Numbers refer to the activation (within parentheses) and reaction energies in kcal mol$^{-1}$.

between reduced and oxidized sites in the $CO/NO/O_2$ system: reactions (7) and/or (8) may dominate reactions (11) and (12), thus limiting the concentration of reduced ZCu sites and shutting off the N–N bond-forming reaction (18). Confirmation of such a mechanism awaits further study of the elementary steps and complex kinetics of $CO/NO/O_2$ reactions.

## 5. Conclusions

First principles density functional theory calculations have been used to study the mechanism of CO oxidation by Cu-exchanged zeolite catalysts. A number of pathways consistent with the known facile oxidation of CO, and involving a variety of unique intermediates, have been identified. In particular, the formation and decomposition of a carbonate intermediate is predicted to contribute to the regeneration of reduced sites. The work provides insight into the non-selective reduction of CO by NO, and represents an important first step towards our goal of obtaining a molecular-level understanding of selective catalytic reduction of NO in Cu-zeolite catalysis.

## Acknowledgement

The authors thank Bryan Goodman for many helpful discussions. DS and JBA also thank NCSA for computational support and Ford Motor Company for financial support.

## References

[1] M. Shelef, Chem. Rev. 95 (1995) 209.
[2] M. Iwamoto and H. Hamada, Catal. Today 10 (1991) 57.
[3] G. Centi and S. Perathoner, Appl. Catal. A 132 (1995) 179.
[4] J.T. Kummer, J. Phys. Chem. 90 (1986) 4747.
[5] N.W. Cant, P.C. Hicks and B.S. Lennon, J. Catal. 54 (1978) 372.
[6] D.R. Rainer, M. Koranne, S.M. Vesecky and D.W. Goodman, J. Phys. Chem. B 101 (1997) 10769.
[7] P.J. Berlowitz, C.H.F. Peden and D.W. Goodman, J. Phys. Chem. 92 (1988) 5213;
D.W. Goodman and C.H.F. Peden, J. Phys. Chem. 90 (1986) 4839;
J. Szanyi and D.W. Goodman, J. Phys. Chem. 98 (1994) 2972.
[8] T. Engel and G. Ertl, Adv. Catal. 28 (1979) 1.
[9] W.F. Schneider, K.C. Hass, R. Ramprasad and J.B. Adams, J. Phys. Chem. B 102 (1998) 3692.
[10] W.F. Schneider, K.C. Hass, R. Ramprasad and J.B. Adams, J. Phys. Chem. B 101 (1997) 4353.
[11] W.F. Schneider, K.C. Hass, R. Ramprasad and J.B. Adams, J. Phys. Chem. 100 (1996) 6032.
[12] K.C. Hass and W.F. Schneider, J. Phys. Chem. 100 (1996) 9292.
[13] K.C. Hass and W.F. Schneider, Phys. Chem. Chem. Phys. (1999) 639.
[14] H.V. Brand, A. Redondo and P.J. Hay, J. Phys. Chem. B 101 (1997) 7691.
[15] Y. Yokomichi, T. Yamabe, H. Ohtsuka and T. Kakumoto, J. Phys. Chem. 100 (1996) 14424;
Y. Yokomichi, H. Ohtsuka, T. Tabata, O. Okada, Y. Yokoi, H. Ishikawa, R. Yamaguchi, H. Matusi, A. Tachibana and Y. Yamabe, Catal. Today 23 (1995) 431.
[16] L. Rodriguez-Santiago, M. Sierka, V. Branchadell, M. Sodupe and J. Sauer, J. Am. Chem. Soc. 120 (1998) 1545.
[17] B.L. Trout, A.K. Chakraborty and A.T. Bell, J. Phys. Chem. 100 (1996) 4173.
[18] B.L. Trout, A.K. Chakraborty and A.T. Bell, J. Phys. Chem. 100 (1996) 17582.
[19] D.J. Liu and J. Robota, in: *Reduction of Nitrogen Oxide Emissions*, ACS Symp. Series, Vol. 587 (Am. Chem. Soc., Washington, DC, 1995) p. 147.
[20] H. Yamashita, M. Matsuoka, K. Tsuji, M. Anpo and M. Che, J. Phys. Chem. 100 (1996) 397.
[21] C. Lamberti, S. Bordiga, M. Salvalaggio, G. Spoto, A. Zecchina, F. Geobaldo, G. Vlaic and M. Bellatreccia, J. Phys. Chem. B 101 (1997) 344.
[22] E.J. Baerends, D.E. Ellis and P. Ross, Chem. Phys. 2 (1973) 41.
[23] A.D. Becke, Phys. Rev. A 38 (1988) 3098.
[24] J.P. Perdew, Phys. Rev. B 33 (1986) 8822.
[25] H.-J. Jang, W.K. Hall and J.L. d'Itri, J. Phys. Chem. 100 (1996) 9416.
[26] T. Beutel, J. Sarkany, G.-D. Lei, J.Y. Yan and W.M.H. Sachtler, J. Phys. Chem. 100 (1996) 845.
[27] Y. Huang, J. Am. Chem. Soc. 95 (1973) 6636.
[28] A.W. Aylor, S.C. Larsen, J.A. Reimer and A.T. Bell, J. Catal. 157 (1995) 592.
[29] G. Spoto, A. Zecchina, S. Bordiga, G. Ricchiardi and G. Matara, Appl. Catal. B 3 (1994) 151.
[30] S. Sakai, K. Kitaura and K. Morokuma, Inorg. Chem. 21 (1982) 760.
[31] R. Caballol, E.S. Macros and J.-C. Barthelat, J. Phys. Chem. 91 (1987) 1328.
[32] K. Nakamoto, *Infrared and Raman Spectra of Inorganic and Coordination Compounds*, 4th Ed. (Wiley, New York, 1986).
[33] M.G. Moll, D.R. Clutter and W.E. Thompson, J. Chem. Phys. 45 (1966) 4469.
[34] A.J. Capote, J.T. Roberts and R.J. Madix, Surf. Sci. 209 (1989) L151.
[35] D. Sengupta, J.B. Adams, W.F. Schneider and K.C. Hass, in preparation.
[36] D. Sengupta, J.B. Adams, W.F. Schneider and K.C. Hass, in preparation.
[37] Q. Cui, K. Morokuma, J.M. Bowman and S.J. Klippenstein, J. Chem. Phys. 110 (1999) 9469.